Elasto-Capillary Manipulation of Freestanding Inorganic Nanosheets: An Implication for Nano-Manufacturing of Low Dimensional Structures

Minhyuk Park[1], Dapeng Li[1], Tianyu Wang[1], Binbin Zhou[1,2], Yang Yang Li[2,3,4,5], Deng Zou[6], Paddy K. L. Chan[6], Yong Yang[1,4,7]*

[1.] Department of Mechanical Engineering, College of Engineering, City University of Hong Kong, Kowloon Tong, Kowloon, Hong Kong SAR 99907, China

[2.]Hong Kong Branch of National Precious Metals Material Engineering Research Centre, City University of Hong Kong, Kowloon Tong, Kowloon, Hong Kong SAR 99907, China

[3.]Center of Super-Diamond and Advanced Films (COSDAF), City University of Hong Kong, Kowloon Tong, Kowloon, Hong Kong SAR 99907, China

[4.]Department of Materials Science and Engineering, College of Engineering, City University of Hong Kong, Kowloon Tong, Kowloon, Hong Kong SAR 99907, China

[5.]Centre for Advanced Structural Materials, Greater Bay Joint Division, Shenyang National Laboratory for Materials Sicence, City University of Hong Kong Shenzhen Research Institue, Shenzhen 518057, China

[6.] Department of Mechanical Engineering, Faculty of Engineering, The University of Hong Kong, Pokfulam Road, Hong Kong SAR 99907, China

[7.] Department of Advanced Design and Systems Engineering, College of Engineering, City University of Hong Kong, Kowloon Tong, Kowloon, Hong Kong SAR 99907, China

* Corresponding authors: Y. Y. (yonyang@cityu.edu.hk)

Abstract

Ultrathin inorganic nanosheets (*e.g.* two-dimensional (2D) nanomaterials, thin films and *etc.*) have been attracting tremendous research interest because of their unique properties and promising applications. However, because of their ultrathin thickness (< 100 nm) and low flexural rigidity, it is difficult to manufacture low dimensional structures using these nanosheets. In this work, we first report the observation of an intriguing elasto-capillary unfolding phenomenon which occurs on a variety of freestanding inorganic nanosheets floating on a liquid surface. Through theoretical modeling and experiments, we demonstrate that one can easily unfold, re-roll and transport different kinds of nanosheets by tuning the interfacial properties of the liquid. As a result, one can assemble nanosheets on the liquid surface into small structures (*e.g.* heterogeneous scrolls, optical resonators) and/or transfer them out of the liquid surface onto other surfaces for the manufacturing of flexible devices. The outcome of our research paves the way for nano-manufacturing of low dimensional structures with ultrathin inorganic nanosheets.

KEYWORDS: capillary force; micro-manufactoring; transfer technique; ultrathin inorganic nanosheets; freestanding nanosheets.

1. Introduction

Since the first discovery of graphene in 2004 [1], 2D nanomaterials have been extensively studied due to their promising applications in biomedical devices[2], optoelectronic devices[3], field-effect transistors[3,4], energy storage[5], and sensing[6]. 2D nanomaterials with atomic- and nano-scale thickness exhibit outstanding physical and chemical properties due to their unique 2D geometric features and electronic structures[7], and have continuously attracted great interest from academia and industry. Nonetheless, controlled manipulation of these 2D nanomaterials poses a general challenge to their applications[8]. To fabricate micro- or nano-devices, 2D nanomaterials need to be purposely structured [8] and transferred [9,10] while any resultant deformation, such as the formation of curvatures and folds [8], could change their electronic and photonic properties. On the other hand, because of their extremely low flexural rigidity, 2D nanomaterials can be easily deformed and/or even damaged by external stimuli (*e.g.* by solid-solid contacts). In addition, the presence of in-plane residual stress often leads to the rolling or twisting of 2D nanomaterials [11,12]. Therefore, it has never been straightforward to manipulate 2D nanomaterials in a controlled manner.

Over the past years, tremendous efforts have been dedicated to structuring and manipulating 2D nanomaterials for real applications. According to the literature[2,8,13–15], the prior works were mainly focused on utilizing internal residual stresses to structure 2D nanomaterials. In doing so, one usually needs to stack multiple different 2D nanomaterials or 2D nanomaterials/ultrathin films (*e.g.* polymer[2], SiO_2[15]) together, which can result in a residual stress gradient in the direction

of thickness. In addition, one has to change the overall temperature[2] or PH[15] of the working environment such that the 2D nanomaterials can be reshaped as a response to the physical/chemical stimuli. Aside from residual stress, surface tension of liquids offers an alternative way to shape/deform 2D nanomaterials[16–19]. For example, a monolayer MoS_2 can be shaped into an origami structure[18] on the curved surface of a liquid droplet (therefore termed as capillary origami [16,17]). Apart from shaping and deformation, we note that the surface of liquids can also help transport 2D and ultrathin materials (*e.g.* graphene[20,21] and polymeric thin films[9]). These findings are interesting; however, we note that the prior methods were based on the shape/morphology of the liquid surface to manipulate 2D or ultrathin materials [17,18], and hinders the further development of liquid-based techniques to manipulate, transport and transfer 2D and ultrathin nanomaterials. In this work, we developed a liquid-based approach to manipulate 2D nanomaterials by considering the balance between the elastic and capillary force acting on them when the 2D nanomaterials are floating on a liquid surface. By systematically altering the surface energy of the liquid, we could easily unfold and/or re-fold freestanding nanosheets, in line with the predictions of the continuum model we proposed. This approach enables facile re-structuring, transfer and assembly of different kinds of nanosheets, which can lead to a variety of applications, such as the construction of organic field-effect transistors (OFET), composite scroll assembly, and tunable optical resonators.

2. Results and Discussion

2.1 Fabrication of Inorganic Nanosheets

For this work, we prepared inorganic (*e.g.* metallic, ceramic *etc.*) nanosheets by the polymer surface buckling enabled exfoliation (PSBEE) method we previously developed [7,22] (please see

Experimental for details). Fig. 1a-f illustrates a typical fabrication process of PSBEE. To begin with, a thin layer of polyvinyl alcohol (PVA) is spin-coated onto the surface of a glass plate (Fig. 1a). After the PVA dries at 80 ℃ for an hour, a thin layer of inorganic film is deposited onto the PVA surface with physical vapor deposition (PVD) (Fig. 1b, c). After that, the film-PVA-glass system is immersed into deionized (DI) water. As the PVA layer swells and buckles with the diffusion of water molecules into it [22], large-sized nanosheets exfoliate from the PVA surface (Fig. 1d-f). By tuning the deposition parameters, such as deposition power and time, we can control the thickness of the nanosheets, which can range from ~10 nm to ~100 nm [7,22] (please see Figure S1 for the thickness characterization of nanosheets fabricated via PSBEE). In addition, we can also control the lateral size and shape of the nanosheets through pre-patterning prior to exfoliation (Fig. 1d). With respect to metallic nanosheets, the lateral size of the metallic nanosheets we fabricated could reach 1 cm and above, which is different from metallic nanosheets synthesized via other methods, such as solution-based chemical synthesis [23–25]. Fig. lg-j show nanosheets of various inorganic materials prepared via PSBEE. Here, it is important to note that PVD may introduce significant residual stress in the nanosheets [22], thus leading to rolling and folding of otherwise flat nanosheets [12,13].

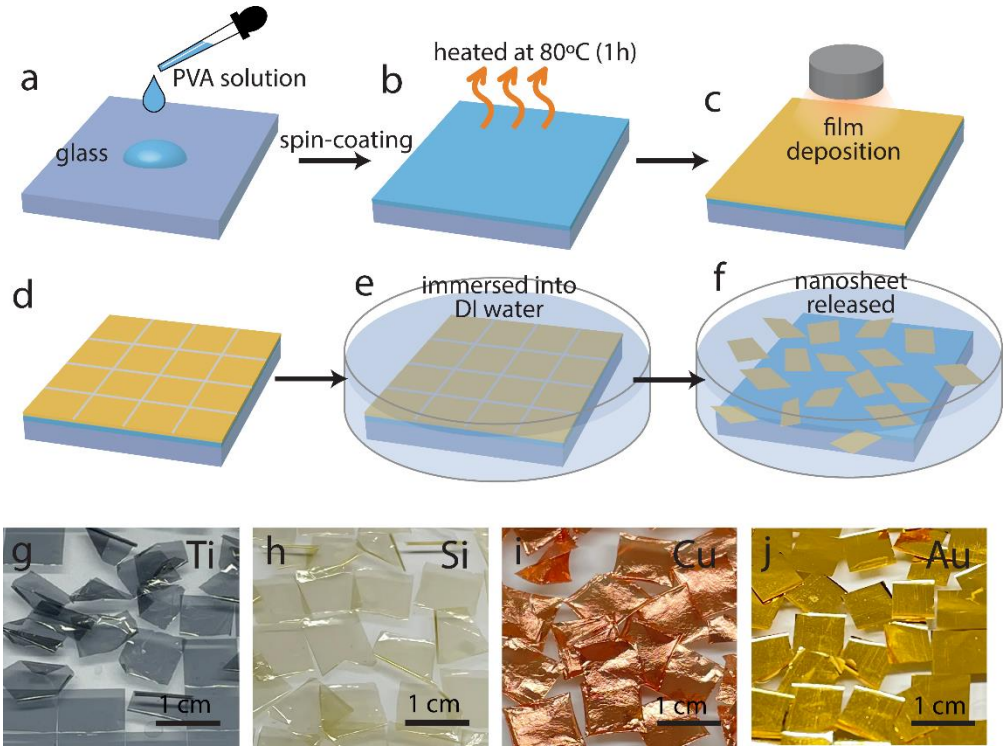

Figure 1. a-f) Schematic illustration of the fabrication of freestanding inorganic nanosheets vis PSBEE, including (a) spin-coating a PVA layer on a glass plate, (b) drying at 60°C for an hour, (c) deposition of a thin layer of inorganic film onto PVA, (d) pre-patterning the deposited film prior to exfoliation, (e) immersion of the film-PVA-glass system into DI water, and (f) exfoliation of the nanosheets. g-j) Photos of nanosheets freely floating in water, composed of (g) Ti, (h) Si (i) Cu, and (j) Au.

2.2 Elasto-Capillary Unfolding: Phenomenon and Theory

Fig. 2a shows a Ti nanosheet self-rolled due to the residual stress effect. Interestingly, under the action of the capillary force, the rolled Ti nanosheet started to unfold once part of it touched the surface of the DI water. Subsequently, the Ti nanosheet was drawn out of the water to its surface (see Movie S1) and continued to unfold itself until the whole nanosheet became fully stretched

while floating atop (Figs. 2b and c). Figs. 2d and e illustrate how unfolding of the rolled nanosheet occurs as the nanosheet-water-air triple junction keeps propagating on the water surface, causing expansion of the unfolded area. Importantly, we could re-roll the unfolded nanosheet by adding surfactants to the water, and repeatedly unfold it on clean water (see Movie S2).

In principle, the capillary enabled unfolding leads to the decrease in the sheet-liquid/liquid-air interfaces and the increase in the sheet-air interface (schematic illustrations in Fig. 2f), which can be attributed to the reduction in the total interfacial energy by U_s. Meanwhile, unfolding of the nanosheet results in elastic bending, hence increasing the elastic energy by U_e. From a thermodynamic viewpoint, spontaneous unfolding occurs when the change in the total free energy $U_e - U_s$ is negative (or $U_e < U_s$). Assuming that the nanosheet has thickness *t*, length *L*, curvature *1/R*, and Young's modulus *E* prior to unfolding, one can derive that $U_e = \frac{B}{2R^2}$, with $B = \frac{Et^3}{12}$ being the bending stiffness per unit width, and $U_s = L(\gamma_{ls} + \gamma_{lv} - \gamma_{sv})$ where γ_{ls}, γ_{lv}, and γ_{sv} denote the interfacial energy between liquid and sheet, liquid and air, and sheet and air, respectively. Substituting the Young's equation $\gamma_{sv} = \gamma_{ls} + \gamma_{lv} \cdot \cos\theta_c$ into the U_s leads to $U_s = L\gamma_{lv}(1 - \cos\theta_c)$ (or the Young-Dupre equation [26]), where θ_c is the equilibrium contact angle between liquid and sheet. In such a case, spontaneous unfolding corresponds to

$$\frac{B}{2R^2} < \gamma_{lv}(1 - \cos\theta_c) \quad (1)$$

Setting $U_e = U_s$, we then derive the critical curvature radius $R_c = \sqrt{\frac{B}{2\gamma_{lv}(1-\cos\theta_c)}}$. Therefore, spontaneous unfolding also corresponds to $R > R_c$. In theory, R_c reaches infinity for $\theta_c = 0°$ (for an extremely hydrophilic sheet) or reaches its minimum for $\theta_c = 180°$ (for an extremely hydrophobic sheet). In other words, unfolding of nanosheet on a liquid surface is favored by hydrophobicity but suppressed by hydrophilicity.

To validate the above thermodynamic theory, we carried out systematic experiments on capillary unfolding of the Ti nanosheets (24nm thick, see Figure S1) on the surface of a water-ethanol solution. The surface tension γ_{lv} of the solution, as a function of the ethanol concentration, was already reported elsewhere[27]. Furthermore, we measured the contact angle of the solution on the Ti nanosheet as a function of the ethanol concentration f_e (weight fraction) from 0% to 22%. As shown in Fig. 2g-i, the contact angle θ_c decreases monotonically with f_e. As a result, all the Ti nanosheets were completely unfolded on the surface of pure water (f_e = 0%) while some of them stayed rolled for a finite f_e (Fig. 2f, insets). We measured all observed radii R from the rolled nanosheets for each ethanol concentration and plot them against $[\gamma_{lv}(1-\cos\theta_c)]^{-1/2}$. According to our theory, the measured radius R should satisfy $R < R_c = \sqrt{\frac{B}{2}}[\gamma_{lv}(1-\cos\theta_c)]^{-1/2}$. In other words, the data in Fig. 2f should be enveloped by the straight line $R = \sqrt{\frac{B}{2}}[\gamma_{lv}(1-\cos\theta_c)]^{-1/2}$, which agrees well with our findings, as seen in Fig. 2f.

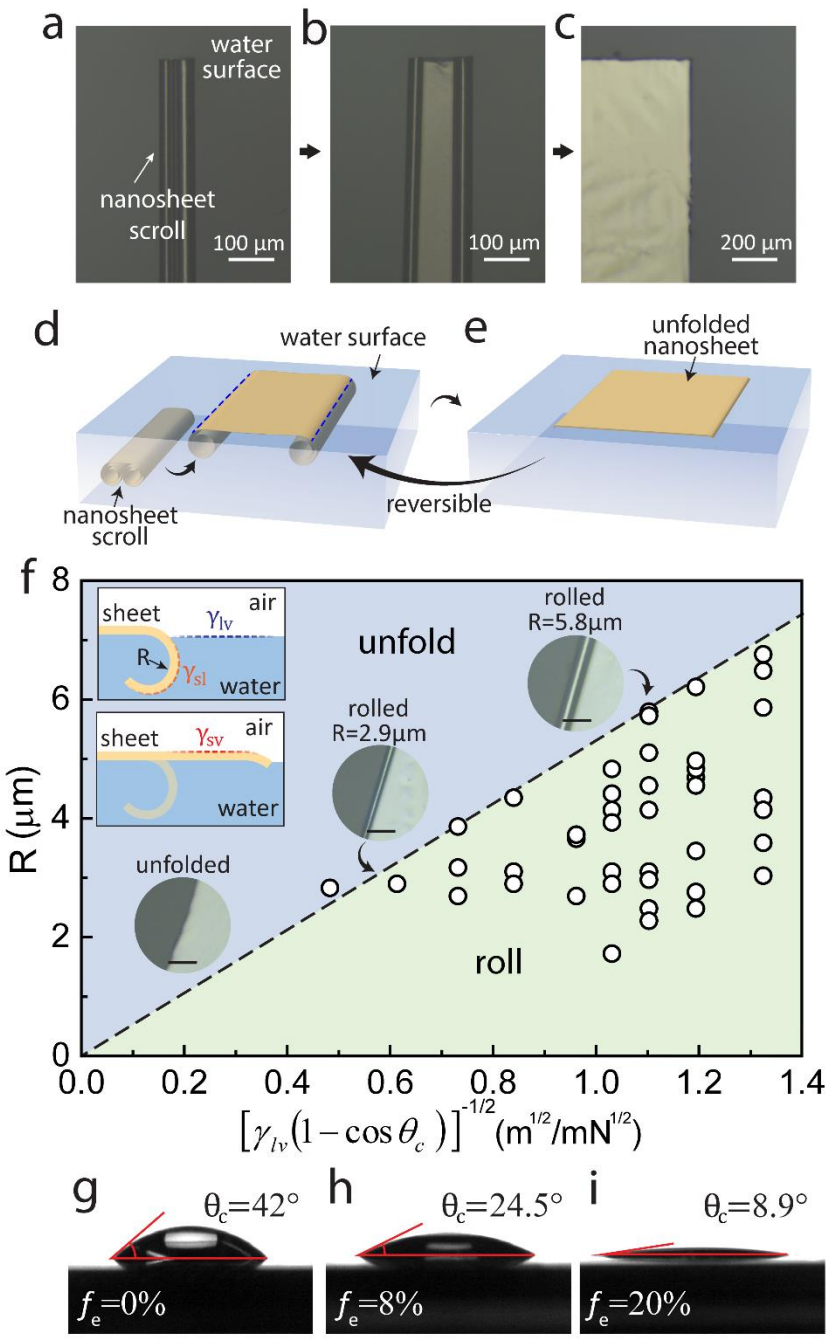

Figure 2. a-c) Optical microscopy images of the unfolding process of a self-rolled Ti nanosheet on the surface of DI water. Observed from below the water surface. d-e) Schematic illustrations of the unfolding process of a nanosheet scroll as it is brought to water surface. A blue dashed line in (d) highlights the nanosheet-water-air triple junction. f) A graph of observed *R* versus [γ_{lv}(1-

$\cos\theta_c)]^{-1/2}$. The dashed line indicates the critical radius R_c proportional to $[\gamma_{lv}(1-\cos\theta_c)]^{-1/2}$. The schematic illustration at upper left shows change of interface energy when a rolled nanosheet is unfolded on the liquid surface, and the insets across the graph show rolled edge of the nanosheet at corresponding $[\gamma_{lv}(1-\cos\theta_c)]^{-1/2}$. Scale bars, 10 μm. g-i) Contact angle of the water-ethanol solution on the surface of the Ti nanosheet with the ethanol concentration of (g) 0%, (h) 8%, and (i) 20%.

Apart from thermodynamics, we further investigate the unfolding mechanics with analytic modeling, which is critical to understanding unfolding of nanosheets during transience. For simplicity, the unfolded part of the nanosheet is considered as the Euler-Bernoulli beam with original curvature 1/*R*, length *L*, and bending stiffness *B*, which is pulled by the capillary force with a magnitude of γ_{lv} at one end and fixed at the other end because of symmetry (Fig. 3a). Meanwhile, the nanosheet is subjected to a hydrostatic pressure distributed over its surface, which can be related to the liquid density ρ and the gravity constant g. Furthermore, we note that dimensional analyses lead to the elasto-capillary length scale $L_{ec} = \sqrt{B/\gamma_{lv}}$ and the elasto-hydrostatic length scale $L_{eh} = (B/\rho g)^{1/4}$ for our problem[28,29]. Therefore, if we assume that the angle between the tangent to the nanosheet and the horizontal (or X) direction is φ (positive if trigonometric) and the arc-length along the nanosheet is S, we can scale length parameters by L_{ec} and obtain the dimensionless lengths $\{s, x, y, r, l, l_{eh}\} = \frac{1}{L_{ec}}\{S, X, Y, R, L, L_{eh}\}$. We therefore derive the following dimensionless governing equations (see Supplementary for the details of derivation):

$$\varphi(s)''' + \frac{1}{2}\varphi'(s)^3 - \cos\theta_a \cdot \varphi'(s) - \frac{1}{2r^2}\varphi'(s) + \frac{1}{l_{eh}{}^4}y(s) = 0 \quad (2a)$$

$$x'(s) = \cos\varphi(s) \quad (2b)$$

$$y'(s) = \sin\varphi(s) \quad (2c)$$

with the boundary conditions

$$x(0) = 0; \varphi(0) = 0; \varphi''(0) = 0 \tag{3a}$$

$$\varphi'(l) = -\frac{1}{r};\ \varphi''(l) = -\sin\theta_a;\ y(l) = -2{l_{eh}}^2 \sin\left[\frac{\theta_a + \varphi(l)}{s}\right] \tag{3b}$$

where θ_a is the angle between the tangent to nanosheet and the liquid surface at the junction (Fig. 3a). Among the dimensionless parameters in the equilibrium equations, l_{eh} (=L_{eh}/L_{ec}) gages the relative importance of the capillary force over the hydrostatic pressure[28]. For our nanosheets, l_{eh} typically ranges from 10^3 to 10^5 ($1/l_{eh}$<<1), which suggests that the effect of hydrostatic pressure is insignificant for our problem. Therefore, unfolding of our nanosheets is governed mainly by the balance between capillarity and elasticity, or more specifically, the dimensionless parameters $r = \frac{R}{L_{ec}}$ and $l = \frac{L}{L_{ec}}$.

By solving Eq. (2) and (3) numerically, we can predict the configuration of an unfolded nanosheet on a liquid surface. Fig. 3b shows a theoretical profile of the unfolded nanosheet obtained at r=4.8, in comparison with the profile of the unfolded NiTi nanosheet on the water surface, which is captured by the Wyko® NT9300 optical profiling system. Evidently, our model shows good agreement with the experimental observation (Fig. 3b). Notably, the edge of the unfolded nanosheet is curved, corresponding to a finite angle θ_a between the nanosheet and the liquid surface (Fig. 3b). From our numerical solutions, we confirm that the r (= $R\gamma_{lv}^{\frac{1}{2}}B^{-\frac{1}{2}}$) dependence of θ_a can be fitted to the relation

$$\cos\theta_a = 1 - 1/(2r^2) \tag{4}$$

when the nanosheet is much larger than the elasto-capillary length (l>>1) (Fig. 3c). Substituting this relation into (1) yields a simple geometric criterion for spontaneous unfolding:

$$\theta_a < \theta_c \tag{5}$$

Fig. 3d shows the variation of θ_a with the dimensionless unfolding length l (= $L\gamma_{lv}^{\frac{1}{2}}B^{-\frac{1}{2}}$) for a number of r values. It is evident that θ_a initially depends on l for a relatively short length (l < 5). As l increases, θ_a rises up and quickly reaches the plateau value θ_a', which is determined by Eq. (4). To generalize our findings, we construct a "phase" diagram of folding versus unfolding, which is characterized by r (= $R\gamma_{lv}^{\frac{1}{2}}B^{-\frac{1}{2}}$) and θ_c (Fig. 3e). The boundary between the "rolled" and "unfolded" phase corresponds to θ_a' = θ_c, which is equivalent to the thermodynamic criterion $R = \sqrt{\frac{B}{2}}[\gamma_{lv}(1-\cos\theta_c)]^{-1/2}$ as indicated in Fig. 2f.

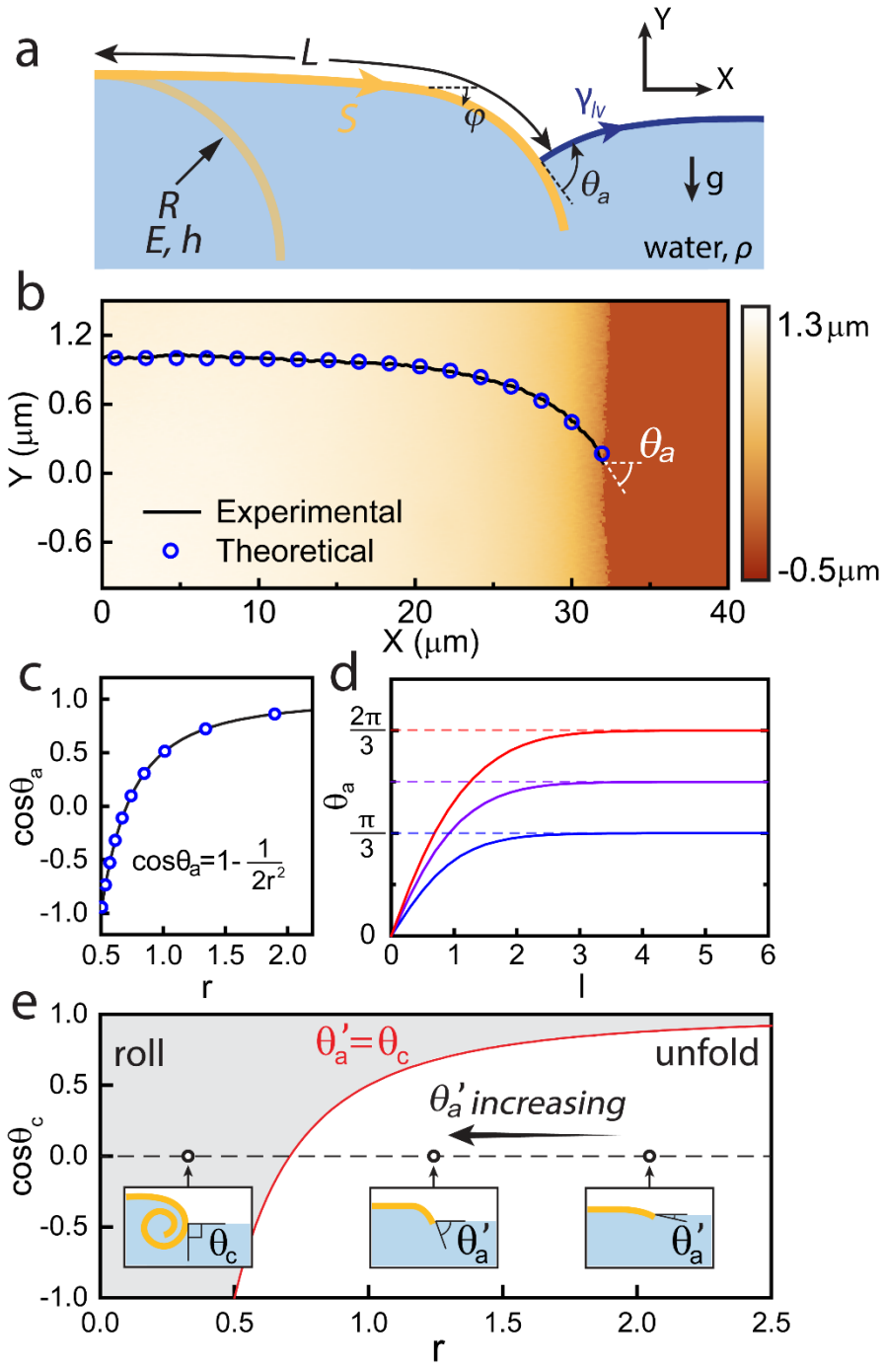

Figure 3. a) A mechanical description for configuration of an unfolded scroll. b) Shape profiles of the unfolded nanosheet obtained by the theoretical model (blue circles), and the experimental observation (black line). The background of the graph shows the optical profiling image of the unfolded nanosheet on water surface, from which the experimental profile (black line) is extracted.

θ_a between the nanosheet and the liquid surface at the junction is marked. c) Numerically computed $\cos\theta_a$ varying with *r* (blue circles), which is fitted to $\cos\theta_a = 1 - \frac{1}{2r^2}$ (black line). d) Numerically computed θ_a varying with *l*. Each curve corresponds to a fixed *r* (from bottom to top, $r = 1, \frac{\sqrt{2}}{2}, \frac{\sqrt{3}}{3}$). e) The unfolding "phase" diagram characterized by the *r* and the balanced contact angle θ_c.

3. Applications

3.1 Elasto-Capillary Enabled Transfer

Aside from its scientific interest, we note that the phenomenon of elasto-capillary unfolding also enables the development of novel methods for manipulating 2D (or ultrathin) nanomaterials. In what follows, we would like to discuss several applications that can be derived from the elasto-capillary unfolding. First, we note that one could obtain fully stretched nanosheets that can facilitate subsequent transfer by unfolding 2D nanosheets on a liquid surface, as exemplified by Figs. 4a-b. The nanosheet unfolded on the liquid surface could be easily transferred onto a rigid substrate (*e.g.* glass) through capillary transfer (Fig. 4c). To do so, we carefully place the glass into the water in the proximity of the nanosheet (*e.g.* 3-4 mm away from the nanosheet). Subsequently, we pull the glass up off the water. As a result of the capillary action, a thin water layer, together with the nanosheet floating on it, is drawn towards and finally sticks onto the substrate, leading to the capillary transfer of the nanosheet. Here, we note that, unlike the transfer of soft thick films (thickness>1 μm) [9], which is based on physical contact between films and a receiver substrate, our method does not need any direct physical contact of nanosheets with the receiver substrate throughout the transfer.

Furthermore, we could transfer the nanosheets onto a "stamp" and subsequently print them onto a target substrate (Fig. 4d-f). As a proof of concept, we fabricated a polydimethylsiloxane (PDMS)

"stamp" (see Experimental) to pick up Au nanosheets through capillary transfer and print it onto target substrates. Given the moderate adhesion between metals and PDMS (*i.e.* ~4J/m^2 for Au/PDMS at a low peeling rate [30]), which is weaker than that between metals and most solid surfaces (*i.e.* >10J/m^2 for Au/Ti [30]), the nanosheet transferred on the stamp could be successfully printed onto various target substrates. As shown in Fig. 4g, we could easily transfer complex-shaped Au nanosheets onto a flexible polyimide (PI) tape with a good control of positioning (Figure S2). Due to the high toughness of the Au nanosheet [31], we can retain the shape of the printed nanosheet. Likewise, we could also transfer the Au nanosheet onto other receiver substrates, such as Si, steel, and polystyrene (Figure S3).

Next, let us estimate the distance d between the nanosheet and the substrate (Fig. 4h), within which the capillary transfer can take place. Due to the capillary force, the profile of the nearby liquid surface is not horizontal but approximately follows the equation $y = c_1 e^{\sqrt{\rho g/\gamma_{lv}}\cdot x}$ before the transfer [32], where y = the height of the liquid surface, x = the distance to the substrate (negative value). In our problem, $c_1 = \sqrt{\frac{\gamma_{lv}}{\rho g}} \cdot \cos\theta_c$, in which ρ = liquid density and g = the gravity constant. After the capillary transfer, force balance requires that the total weight of the nanosheet and the liquid layer, as indicated by the red area in Fig. 4h, should be smaller than the vertical component of the capillary force $\gamma_{lv}\cos\theta_c$. Therefore, we can derive (see Supplementary for details):

$$d \leq \sqrt{\frac{\gamma_{lv}}{\rho g}} \cdot \ln\left(\frac{\gamma_{lv}\cos\theta_c}{\rho_s g h L}\right) \quad (6)$$

where ρ_s, h, and L denote the density, thickness and length of the nanosheet respectively. Taking γ_{lv} = 72 mN/m, $\gamma_{lv}\cos\theta_c$ =30 mN/m, ρ = 10^3 N/m^3, ρ_s = 10^4 kg/m^3, h = 10 nm and L = 8 mm, we estimate that the maximum distance that allows capillary transfer should be around 1 cm, which agrees fairly well with our experimental observations.

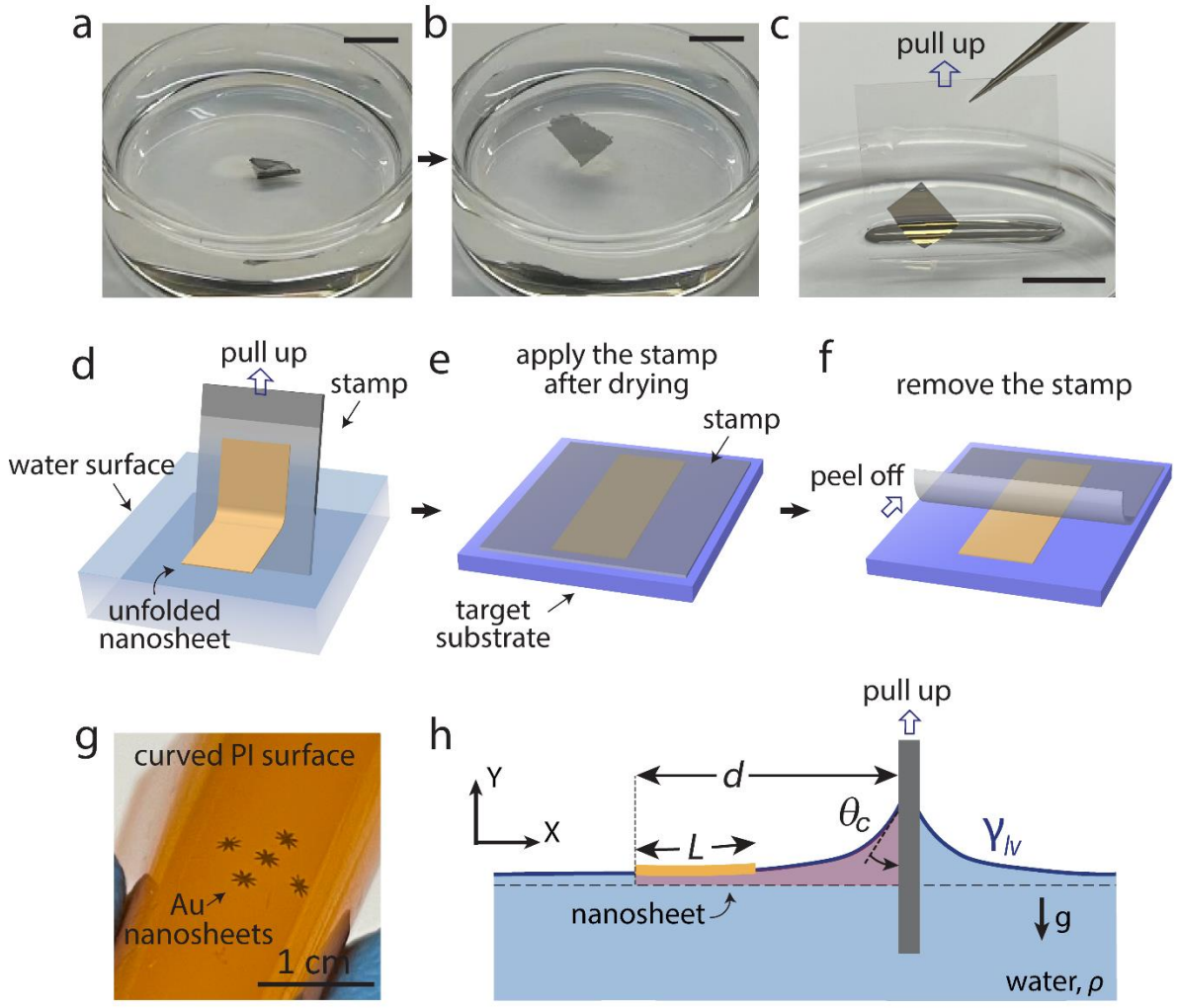

Figure 4. a-c) Photos of (a) the Ti nanosheet freely floating under water with large deformations, (b) the Ti nanosheet unfolded on the surface of water, and (c) capillary transfer of the Ti nanosheet onto a glass slide, where the glass slide is pulled up off the water. Scale bars, 1 cm. d-f) Schematic illustrations of the transfer process, including (d) transfer an unfolded nanosheet onto the stamp through capillary transfer, (e) apply the stamp onto the target substrate with the nanosheet facing the substrate, and (f) peel off the stamp. g) Complex-shaped Au nanosheets printed onto a flexible PI tape. h) 2D description of the capillary transfer of the nanosheet, schematic illustration.

3.2 Conformable Electrode

Based on the above findings, we can make a metallic nanosheet (*e.g.* Au) a conformable electrode (size 40μm×200μm) by capillary-transferring it onto an organic field-effect transistor (OFET), where monolayer crystals of organic semiconductor (OSC) (2,9-didecyldinaphtho[2,3-b:2′,3′-f]thieno[3,2-b]thiophene (C10-DNTT)) were employed as the active layer [4]. For such a thin crystal OSC active layer, a nondestructive integration of electrode is desirable, thereby excluding direct deposition of electrodes because of the potential damage on the OSC layer [4]. Therefore, our capillary transfer method becomes attractive, which allows us to transfer ultrathin (~20 nm thick, Fig. S1) Au electrodes onto the OSC layers undamaged. As shown in Fig. 5a, an ultrathin Au nanosheet was successfully transferred onto the OFET as a source electrode with a conformal physical contact with the OSC layer, in comparison with a thick Au film (180 nm thick) drain electrode transferred through mechanical "pick-and-place" method [4] (Experimental). With the present transfer method, we could easily set the channel width (W) and length (L) to be 200 μm and 10 μm, respectively. Figs. 5b and c show the transfer curves and output curves of the OFET obtained through the capillary transfer of an ultrathin Au nanosheet. Compared to the previous OFET with mechanically transferred Au films as the electrodes[4] (Fig. 5d, e), our OFET with a capillary transferred source electrode shows a higher width-normalized drain-source current (I_{DS}/W), reaching 5.6 μA μm^{-1} (44.4% higher) at a drain-source voltage V_{DS}=-80 V.

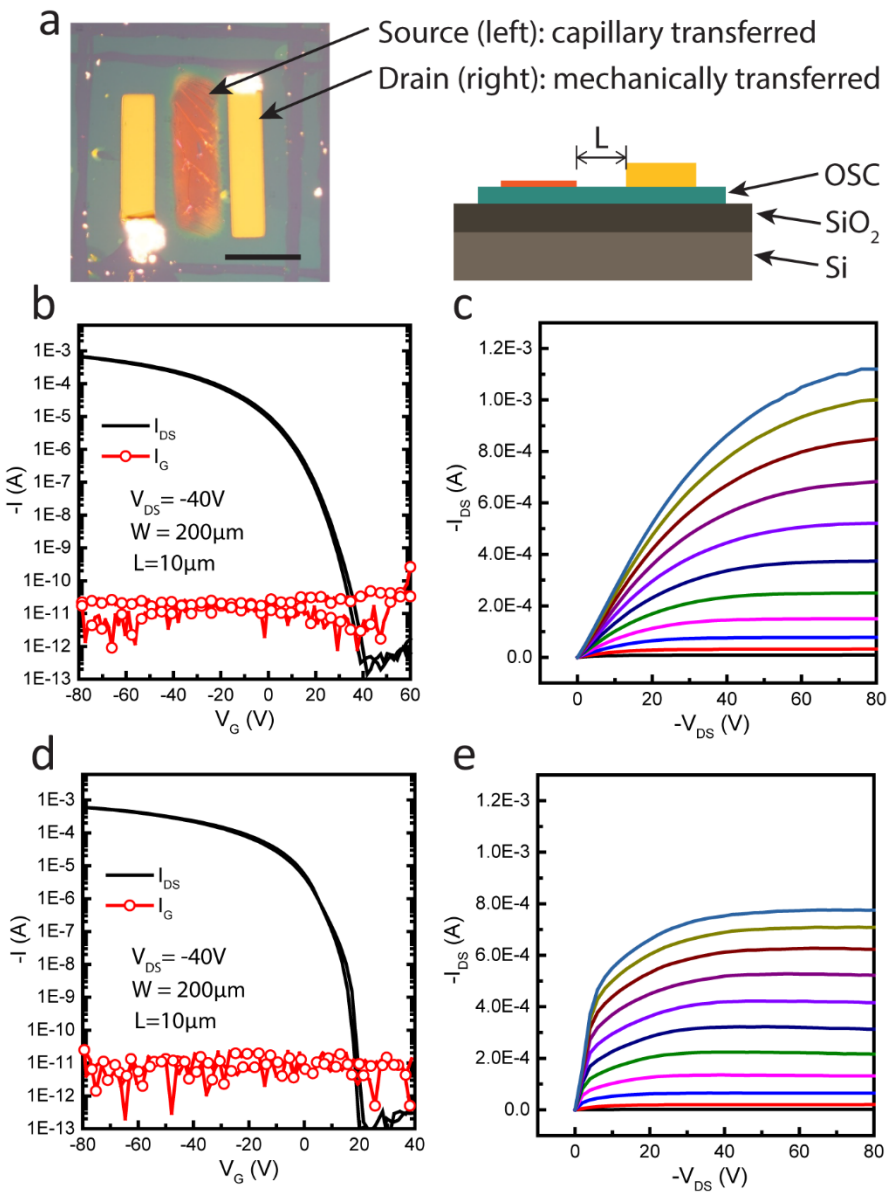

Figure 5. a) An optical microscopy image (left) and a schematic cross-section (right) of the OFET based on 1L-crystal OSC. The source electrode is capillary transferred while the drain electrode is transferred by the traditional mechanical method, placed left and right respectively in the images. Scale bar, 100 µm. b) Transfer curves of the device at V_{DS} = -40 V. c) Output curves of the device scanned from V_G = 0 V to -100 V, with a step size of -10 V. d,e) Curves obtained from an OFET with electrodes (source and drain) all composed of regular Au films. d) Transfer curves of the

device at V_{DS} = -40 V. e) Output curves of the device scanned from V_G = 0 V to -100 V, with a step size of -10 V.

3.3 Controlled Assembly of Scrolled Nanosheets

Apart from capillary transfer, we can assemble two nanosheets into a composite scroll by unfolding and re-rolling the nanosheets on the surface of a same liquid (*e.g.* NiTi and Si as seen Fig. 6b), as sketched in Fig. 6a. Here, we note that the two nanosheets are bonded through van der Waals (vdW) forces on the water surface, leading to surface wrinkling as discussed in Ref.[33]. After we reduced the surface energy $\gamma_{lv}(1-\cos\theta_c)$ through the addition of surfactants (sodium dodecyl sulfate) into the water, the two nanosheets rolled together into a composite scroll, as seen in Fig. 6c. Alternatively, we can also produce a composite scroll by wrapping a scroll with a nanosheet, as illustrated in Fig. 6d. Fig. 6e shows a NiTi nanosheet unfolded on the liquid surface with a nanosheet scroll (Ti) underneath. Likewise, by tuning the surface energy of the liquid, we rolled the upper nanosheet such that it completely wrapped around the scroll underneath (Fig. 6f and Figure S4). In principle, we can fabricate different composite scrolls by combining different nanosheets through concomitant rolling or wrapping (Fig. 6g-j). These composite scrolls are interesting and analogous to the vdW superlattice structures reported in the literature [34,35], the latter of which have shown a great potential of applications in various fields, such as transistors and quantum tunneling devices[35,36]. Given its convenience and versatility, the elasto-capillary unfolding method herein developed provides a flexible approach to assemble micro-structures and functional vdW composite scrolls, which can be hardly fabricated otherwise.

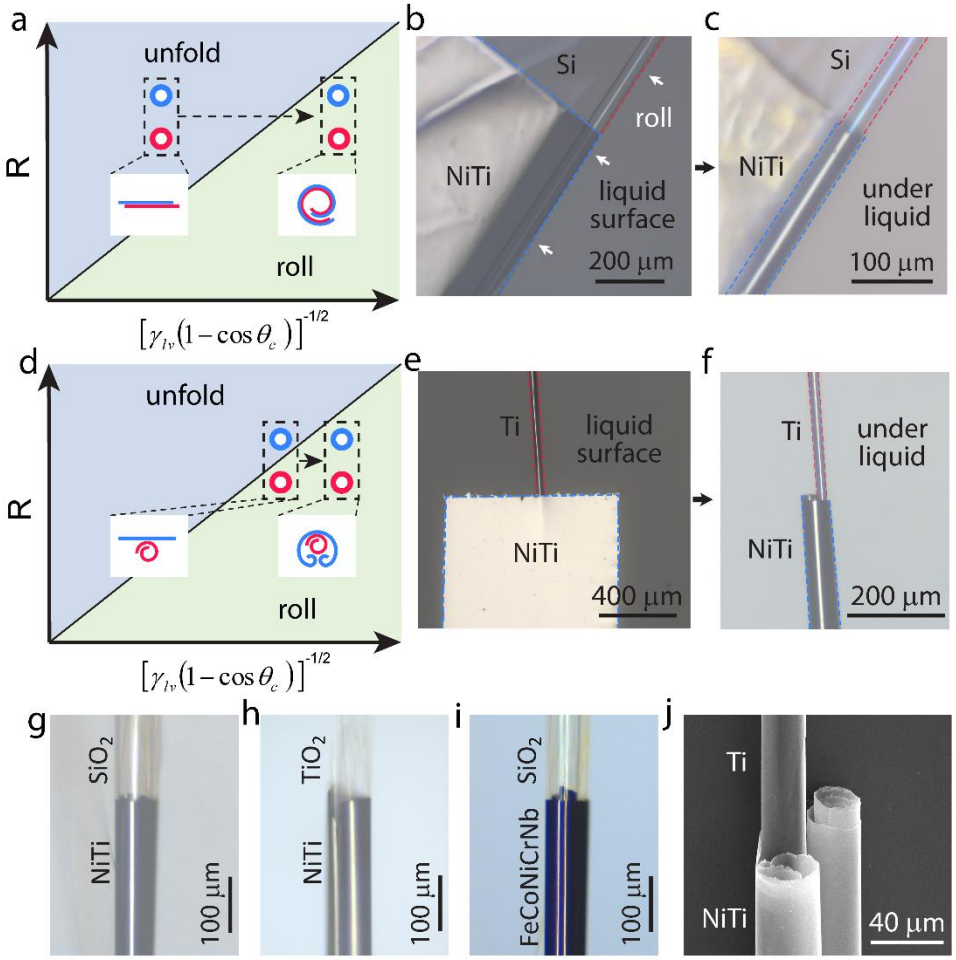

Figure 6. a) Schematic illustration of the phase transition during assembly. b) A NiTi nanosheet and a Si nanosheet rolling together on the liquid surface. c) A composite scroll formed by the concomitant rolling. d) Schematic illustration of the phase transition during assembly (wrapping). e) A NiTi nanosheet unfolded on the water surface with a Ti nanosheet scroll arranged underneath. f) A composite scroll formed by wrapping the underneath scroll with a nanosheet. g-i) Composite scrolls formed by rolling nanosheets, composed of (g) NiTi+SiO_2, (h) NiTi+TiO_2, and (i) FeCoNiCrNb+SiO_2. j) A scanning electron microscope (SEM) images of a composite scroll formed by wrapping a Ti nanosheet scroll with a NiTi nanosheet.

3.4 Tunable Optical Resonator

Finally, we demonstrate the fabrication of a tunable optical resonator through the elasto-capillary unfolding/re-rolling of Si/SiO_x nanosheets prepared by PSBEE. Following Refs.[34,37,38], we annealed our Si/SiO_x nanosheet scrolls for 1 h at 1000 ^{0}C prior to photoluminescence experiments. As seen in Fig. 7, we could unfold the annealed Si/SiO_x nanosheet on the surface of water, which showed a rather weak optical resonant mode at the energy of ~2 eV in its photoluminescence spectrum obtained under the excitation by 514-nm laser at room temperature (see Experimental). In contrast, the rolled state of the Si/SiO_x nanosheet exhibited numerous pronounced optical resonant modes in its photoluminescence spectrum (Fig. 7). These interesting results echo well with the prior findings[11,39] that optical resonanance is sensitive to the morphology of micro-scrolls and demonstrate that the elasto-capillary unfolding method herein developed is versatile and convenient to make such tunable optical resonators. According to the literature[11,39–41], such a optical resonantor could have a broad range of applications (*e.g.* optofluidics and optical signal processing), which is worth further investigation.

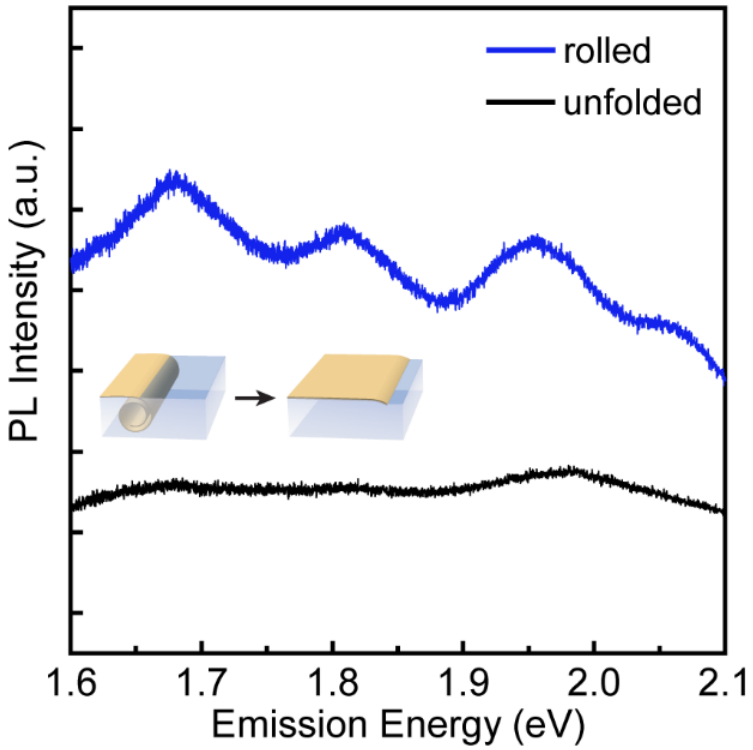

Figure 7. Photoluminescence spectra of the optical resonator (Si/SiO_x bilayer scroll) as it is rolled (blue line) and unfolded (black line). The insets (schematic illustrations) show rolled and unfolded state of the Si/SiO_x nanosheet.

4. Summary

In summary, we studied the elasto-capillary unfolding phenomenon in this work through theoretical modeling and systematic experiments, which enabled us to reshape and manipulate ultrathin nanosheets on a liquid surface in a controlled manner. Compared to the prior methods that were reported in the literature[17–19], the elasto-capillary enabled manipulation of nanosheets is convenient, fast and versatile, which can lead to many applications. As a proof of concept, we demonstrate the capillary transfer of freestanding gold nanosheets to make conformable electrodes

of OFET, the assembly of rolled nanosheets for composite scrolls, and the fabrication of tunale optical ring resonators. These demonstrations deliver a strong message that the elasto-capillary manipulation of freestanding inorganic nanosheets could have a promising future in different fields, from micromotors[42], on-chip electronics[3] to sensing[43].

5. Experimental

Polymer surface buckling enabled exfoliation (PSBEE): Polyvinyl alcohol (PVA) solution of 11 wt% was prepared by dissolving PVA 0588 powder (99%, Shanghai Chenqi Chemical Technology Co., Ltd) in water at 40℃. After the PVA was completely dissolved and cooled down to room temperature (RT), the solution was spin-coated onto glass plates (spin rate 2000 rpm, spin time 40 s), and then dried for an hour under the temperature of 80 ℃ in a drying oven. Subsequently, a thin layer of inorganic film was deposited onto the PVA surface via physical vapor deposition (PVD). After deposition, the film-PVA-glass system was immersed into water, then the inorganic nanosheets were exfoliated from the substrate within minutes.

Deposition of inorganic films for fabrication of nanosheets: Deposition of NiTi, FeCoNiCrNi, Si, SiO_2, and TiO_2 was carried out by magnetron sputtering system, utilizing corresponding targets. The chamber pressure was under 1×10^{-5} Torr. Ar gas (99.9%) was introduced as working gas with the flow rate and working pressure of 20 sccm and 10 mTorr, respectively. We used direct current (DC) to deposit metals (NiTi, FeCoNiCrNi), and radio frequency (RF) to deposit other materials (Si, SiO_2, TiO_2). Deposition power and the time varied by different materials and desired sheet thickness, ranging from 50-150W and 200-1000s. Deposition of Ti and Cu was carried out by an e-beam evaporator under high vacuum ($< 6\times10^{-6}$ Pa), with a deposition rate of 1 Å/s. Au film was

deposited by ion beam sputtering (JEOL JHC-1100E ion sputter) under the working pressure 10^{-1} Pa, and the direct current 10 mA. Shadow masks were applied in deposition to shape the Au film into an electrode (40×200 μm) or a flower-like pattern (radius 500 μm).

Preparation of polydimethylsiloxane (PDMS) stamp: Sylgard 184 pre-polymer and curling agent (Dow Inc.) are mixed with a weight ratio of 10:1. After mixing them for a couple of minutes (~10 min), we pour the mixture slowly into a plastic mold. The mold containing the mixture (PDMS) was placed in an oven and cured at 70℃ for 4 hours. After the PDMS was fully cured, we took out the mold from the oven and wait until the sample is cooled down. Then we slowly separated the PDMS from the plastic mold.

Mechanical transfer of Au electrodes: In this method, the Au electrodes (180 nm thick) were deposited on OTS-treated SiO_2/Si wafer by thermal evaporation. Shadow masks were used in deposition to form rectangular electrodes with size of 40×200 μm. After deposition, a CuBe probe equipped on a microscope was used to stick and lift one end of the Au electrode. Due to rigidity of the Au electrode, the whole electrode was slowly lift off by the probe. Then the Au electrode on the probe was carefully placed onto the surface of OSC.

Measurement of photoluminescence (PL) spectra: The PL spectra of the rolled and unfolded Si/SiO_x nanosheet were acquired at room temperature by a Renishaw inVia Raman microscope with the laser wavelength of 514 nm. The laser power and the acquisition time were 17 mW and 1 s respectively.

ASSOCIATED CONTENT

Supplementary materials

The following files are available free of charge.

Thickness characterization of inorganic nanosheets prepared via PSBEE, transfer an printing porcess of shaped Au nanosheets onto PI tape, printing of Au nanosheet electrodes onto various substrates, SEM image and composition mapping of the composite scroll formed by “wrapping,, assembly, derivation of the equilibrium equations for the elasto-capillary unfolding, derivation of th transfer distance (PDF)

Supplementary Movie S1 Unfolding of a Ti nanosheet scroll on the water surface (MP4)

Supplementary Movie S2 Re-rolling and repeated unfolding of the nanosheet (MP4)

AUTHOR INFORMATION

Corresponding Author

*Yong Yang (yonyang@cityu.edu.hk)

Present Addresses

Department of Mechanical Engineering, College of Engineering, City University of Hong Kong, Kowloon Tong, Kowloon, Hong Kong SAR 99907, China; Department of Materials Science and Engineering, College of Engineering, City University of Hong Kong, Kowloon Tong, Kowloon, Hong Kong SAR 99907, China; Department of Advanced Design and Systems Engineering, College of Engineering, City University of Hong Kong, Kowloon Tong, Kowloon, Hong Kong SAR 99907, China

Author Contributions

The manuscript was written through contributions of all authors. All authors have given approval to the final version of the manuscript.

ACKNOWLEDGMENT

The work of Y.Y. is supported by the Research Grants Council (RGC), the Hong Kong government, through the General Research Fund (GRF) with the grant numbers CityU11200719 and CityU11213118 and through the NSCF-RGC joint research scheme with the grant number N_CityU 109/21.

References

[1] I.V.G. and A.A.F. K. S. Novoselov, A. K. Geim, S. V. Morozov, D. Jiang, Y. Zhang, S. V. Dubonos, Electric Field Effect in Atomically Thin Carbon Films, 306 (2016) 666–669.

[2] W. Xu, Z. Qin, C.-T.T. Chen, H.R. Kwag, Q. Ma, A. Sarkar, M.J. Buehler, D.H. Gracias, Ultrathin thermoresponsive self-folding 3D graphene, Sci. Adv. 3 (2017) e1701084. https://doi.org/10.1126/sciadv.1701084.

[3] T. Deng, Z. Zhang, Y. Liu, Y. Wang, F. Su, S. Li, Y. Zhang, H. Li, H. Chen, Z. Zhao, Y. Li, Z. Liu, Three-Dimensional Graphene Field-Effect Transistors as High-Performance Photodetectors, Nano Lett. 19 (2019) 1494–1503. https://doi.org/10.1021/acs.nanolett.8b04099.

[4] B. Peng, K. Cao, A.H.Y. Lau, M. Chen, Y. Lu, P.K.L. Chan, Crystallized Monolayer Semiconductor for Ohmic Contact Resistance, High Intrinsic Gain, and High Current Density, Adv. Mater. 32 (2020) 1–9. https://doi.org/10.1002/adma.202002281.

[5] B. Anasori, M.R. Lukatskaya, Y. Gogotsi, 2D metal carbides and nitrides (MXenes) for energy storage, Nat. Rev. Mater. 2 (2017). https://doi.org/10.1038/natrevmats.2016.98.

[6] L. Surface, P. Resonance, S.R. Beeram, F.P. Zamborini, Purification of Gold Nanoplates Grown, 4 (2010) 3633–3646.

[7] T. Wang, M. Park, Q. Yu, J. Zhang, Y. Yang, Stability and synthesis of 2D metals and alloys: a review, Mater. Today Adv. 8 (2020) 100092. https://doi.org/10.1016/j.mtadv.2020.100092.

[8] Z. Zhang, Z. Tian, Y. Mei, Z. Di, Shaping and structuring 2D materials via kirigami and origami, Mater. Sci. Eng. R Reports. 145 (2021) 100621. https://doi.org/10.1016/j.mser.2021.100621.

[9] Y. Zhang, M. Yin, Y. Baek, K. Lee, G. Zangari, L. Cai, B. Xu, Capillary transfer of soft films, Proc. Natl. Acad. Sci. U. S. A. 117 (2020) 5210–5216. https://doi.org/10.1073/pnas.2000340117.

[10] C. Linghu, S. Zhang, C. Wang, J. Song, Transfer printing techniques for flexible and stretchable inorganic electronics, Npj Flex. Electron. 2 (2018). https://doi.org/10.1038/s41528-018-0037-x.

[11] Y. Mei, G. Huang, A.A. Solovev, E.B. Ureña, I. Mönch, F. Ding, T. Reindl, R.K.Y. Fu, P.K. Chu, O.G. Schmidt, Versatile approach for integrative and functionalized tubes by strain engineering of nanomembranes on polymers, Adv. Mater. 20 (2008) 4085–4090. https://doi.org/10.1002/adma.200801589.

[12] T. Wang, Z. Zhang, M. Park, Q. Yu, Y. Yang, Etching-Free Ultrafast Fabrication of Self-

Rolled Metallic Nanosheets with Controllable Twisting, Nano Lett. 21 (2021) 7159–7165. https://doi.org/10.1021/acs.nanolett.1c01789.

[13] M. Park, T. Wang, J. Zhang, Q. He, Q. Yu, Y. Yang, Self-Constructed micro-origami of 2D metal, Appl. Mater. Today. 23 (2021) 101039. https://doi.org/10.1016/j.apmt.2021.101039.

[14] E.A. Peraza-Hernandez, D.J. Hartl, R.J. Malak, D.C. Lagoudas, Origami-inspired active structures: A synthesis and review, Smart Mater. Struct. 23 (2014). https://doi.org/10.1088/0964-1726/23/9/094001.

[15] M.Z. Miskin, K.J. Dorsey, B. Bircan, Y. Han, D.A. Muller, P.L. McEuen, I. Cohen, Graphene-based bimorphs for micron-sized, tautonomous origami machines, Proc. Natl. Acad. Sci. U. S. A. 115 (2018) 466–470. https://doi.org/10.1073/pnas.1712889115.

[16] B. Roman, J. Bico, Elasto-capillarity: Deforming an elastic structure with a liquid droplet, J. Phys. Condens. Matter. 22 (2010). https://doi.org/10.1088/0953-8984/22/49/493101.

[17] C. Py, P. Reverdy, L. Doppler, J. Bico, B. Roman, C.N. Baroud, Capillary origami: Spontaneous wrapping of a droplet with an elastic sheet, Phys. Rev. Lett. 98 (2007) 2–5. https://doi.org/10.1103/PhysRevLett.98.156103.

[18] M.F. Reynolds, K.L. McGill, M.A. Wang, H. Gao, F. Mujid, K. Kang, J. Park, M.Z. Miskin, I. Cohen, P.L. McEuen, Capillary Origami with Atomically Thin Membranes, Nano Lett. 19 (2019) 6221–6226. https://doi.org/10.1021/acs.nanolett.9b02281.

[19] T.G. Leong, P.A. Lester, T.L. Koh, E.K. Call, D.H. Gracias, Surface tension-driven self-folding polyhedra, Langmuir. 23 (2007) 8747–8751.

[20] I. Jeon, M.D. Peeks, S. Savagatrup, L. Zeininger, S. Chang, G. Thomas, W. Wang, T.M. Swager, Janus Graphene: Scalable Self-Assembly and Solution-Phase Orthogonal Functionalization, Adv. Mater. 31 (2019) 1–7. https://doi.org/10.1002/adma.201900438.

[21] G. Zhang, A.G. Güell, P.M. Kirkman, R.A. Lazenby, T.S. Miller, P.R. Unwin, Versatile Polymer-Free Graphene Transfer Method and Applications, ACS Appl. Mater. Interfaces. 8 (2016) 8008–8016. https://doi.org/10.1021/acsami.6b00681.

[22] T. Wang, Q. He, J. Zhang, Z. Ding, F. Li, Y. Yang, The controlled large-area synthesis of two dimensional metals, Mater. Today. (2020). https://doi.org/10.1016/j.mattod.2020.02.003.

[23] M. Maillard, S. Giorgio, M.P. Pileni, Tuning the size of silver nanodisks with similar aspect ratios: Synthesis and optical properties, J. Phys. Chem. B. 107 (2003) 2466–2470. https://doi.org/10.1021/jp022357q.

[24] C. Salzemann, J. Urban, I. Lisiecki, M.P. Pileni, Characterization and growth process of copper nanodisks, Adv. Funct. Mater. 15 (2005) 1277–1284. https://doi.org/10.1002/adfm.200400594.

[25] Y. Xiong, I. Washio, J. Chen, H. Cai, Z.-Y. Li, Y. Xia, Poly(vinyl pyrrolidone): A Dual Functional Reductant and Stabilizer for the Facile Synthesis of Noble Metal Nanoplates in Aqueous Solutions, Langmuir. 22 (2006) 8563–8570. https://doi.org/10.1021/la061323x.

[26] M.E. Schrader, Young-Dupre Revisited, Langmuir. 9 (1995) 3585–3589.

[27] G. Vazquez, E. Alvarez, J.M. Navaza, Surface Tension of Alcohol + Water from 20 to 50 °C, J. Chem. Eng. Data. 40 (1995) 611–614. https://doi.org/10.1021/je00019a016.

[28] M. Rivetti, A. Antkowiak, Elasto-capillary meniscus: Pulling out a soft strip sticking to a liquid surface, Soft Matter. 9 (2013) 6226–6234. https://doi.org/10.1039/c3sm50251a.

[29] J. Bico, B. Roman, L. Moulin, A. Boudaoud, Elastocapillary coalescence in wet hair, Nature. 432 (2004) 690. https://doi.org/10.1038/432690a.

[30] X. Feng, M.A. Meitl, A.M. Bowen, Y. Huang, R.G. Nuzzo, J.A. Rogers, Competing fracture in kinetically controlled transfer printing, Langmuir. 23 (2007) 12555–12560. https://doi.org/10.1021/la701555n.

[31] Q. Yu, J. Zhang, J. Li, T. Wang, M. Park, Q. He, Z. Zhang, Strong, Ductile, and Tough Nanocrystal-Assembled Freestanding Gold Nanosheets, Nano Lett. (2022). https://doi.org/10.1021/acs.nanolett.1c04553.

[32] B.E. Rapp, Microfluidics: modeling, mechanics and mathematics, William Andrew, 2016.

[33] S. Deng, V. Berry, Wrinkled, rippled and crumpled graphene: An overview of formation mechanism, electronic properties, and applications, Mater. Today. 19 (2016) 197–212. https://doi.org/10.1016/j.mattod.2015.10.002.

[34] R. Songmuang, A. Rastelli, S. Mendach, O.G. Schmidt, SiOx/Si radial superlattices and microtube optical ring resonators, Appl. Phys. Lett. 90 (2007). https://doi.org/10.1063/1.2472546.

[35] B. Zhao, Z. Wan, Y. Liu, J. Xu, X. Yang, D. Shen, Z. Zhang, C. Guo, Q. Qian, J. Li, R. Wu, Z. Lin, X. Yan, B. Li, Z. Zhang, B. Li, X. Chen, Y. Qiao, I. Shakir, Z. Almutairi, F. Wei, Y. Zhang, X. Pan, Y. Huang, Y. Ping, X. Duan, X. Duan, High-order superlattices by rolling up van der Waals heterostructures, 591 (2021). https://doi.org/10.1038/s41586-

021-03338-0.

[36] B. Xu, X. Lin, Y. Mei, Versatile Rolling Origami to Fabricate Functional and Smart Materials, Cell Reports Phys. Sci. 1 (2020) 100244. https://doi.org/10.1016/j.xcrp.2020.100244.

[37] L.X. Yi, J. Heitmann, R. Scholz, M. Zacharias, Si rings, Si clusters, and Si nanocrystals - Different states of ultrathin SiOx layers, Appl. Phys. Lett. 81 (2002) 4248–4250. https://doi.org/10.1063/1.1525051.

[38] D. Nesheva, C. Raptis, A. Perakis, I. Bineva, Z. Aneva, Z. Levi, S. Alexandrova, H. Hofmeister, Raman scattering and photoluminescence from Si nanoparticles in annealed SiO x thin films, J. Appl. Phys. 92 (2002) 4678–4683. https://doi.org/10.1063/1.1504176.

[39] G.S. Huang, S. Kiravittaya, V.A. Bolaños Quiñones, F. Ding, M. Benyoucef, A. Rastelli, Y.F. Mei, O.G. Schmidt, Optical properties of rolled-up tubular microcavities from shaped nanomembranes, Appl. Phys. Lett. 94 (2009) 1–4. https://doi.org/10.1063/1.3111813.

[40] R. Songmuang, A. Rastelli, S. Mendach, C. Deneke, O.G. Schmidt, From rolled-up Si microtubes to SiOx/Si optical ring resonators, Microelectron. Eng. 84 (2007) 1427–1430. https://doi.org/10.1016/j.mee.2007.01.089.

[41] P. Song, C. Chen, J. Qu, P. Ou, M.H.T. Dastjerdi, Z. Mi, J. Song, X. Liu, Rolled-up SiOx/SiNx microtubes with an enhanced quality factor for sensitive solvent sensing, Nanotechnology. 29 (2018). https://doi.org/10.1088/1361-6528/aad0b1.

[42] S.K. Srivastava, M. Guix, O.G. Schmidt, Wastewater Mediated Activation of Micromotors for Efficient Water Cleaning, Nano Lett. 16 (2016) 817–821.

https://doi.org/10.1021/acs.nanolett.5b05032.

[43] X. Lin, Y. Fang, L. Zhu, J. Zhang, G. Huang, J. Wang, Y. Mei, Self-Rolling of Oxide Nanomembranes and Resonance Coupling in Tubular Optical Microcavity, Adv. Opt. Mater. 4 (2016) 936–942. https://doi.org/10.1002/adom.201500776.